Albero-Sancho, J.; Vidal, A.; Migani, A.; Concepción Heydorn, P.; Blancafort, L.; García Gómez, H. (2019). Phosphorus-Doped Graphene as a Metal-Free Material for Thermochemical Water Reforming at Unusually Mild Conditions. ACS Sustainable Chemistry & Engineering. 7(1):838-846. https://doi.org/10.1021/acssuschemeng.8b04462

Phosphorous-doped graphene as a metal-free material for thermochemical water reforming at unusually mild conditions

Josep Albero,† Alfonso Vidal,‡ Annapaola Migani,§ Patricia Concepción,† Lluís Blancafort § and Hermenegildo García†**

† Instituto Universitario de Tecnología Química CSIC-UPV, Universitat Politècnica de València, Av. De los Narajos s/n, 46022, Valencia, Spain. E-mail: hgarcia@qim.upv.es

‡ CIEMAT-PSA, Avda.complutense, 40, 28040, Madrid, Spain.

§ Institut de Química Computacional i Catàlisi and Departament de Química, Facultat de Ciències, Universitat de Girona, C/ M A. Company 69, 17003 Girona, Spain. E-mail: lluis.blancafort@udg.edu

KEYWORDS

graphene, phytic acid, thermocatalysis, water reforming, metal-free catalyst.

ABSTRACT

P-doped graphene (Phy-G) prepared by pyrolysis of phytic acid at 900 ºC under inert atmosphere has been evaluated as metal-free catalyst for the thermochemical water splitting. XPS, solid-state ^{31}P-NMR and Raman spectroscopy confirm the presence of P atoms bonded to C atoms in the graphene lattice as well as some oxygenated P groups, such as phosphates or phosphonates. HRTEM and AFM images show the characteristic sheet morphology of 2D graphene materials of several micrometers lateral size and exhibiting a high crystallinity with the characteristic hexagonal arrangement of graphenic materials. Phy-G has been submitted to consecutive oxidation/activation thermochemical cycles at 650 and 800 ºC under H_2O-saturated Ar and Ar atmospheres, respectively. During the oxidation periods, H_2 evolution up to 21.6 μmol/min·g was measured. However, no O_2 evolves in the activation steps. Experimental evidence and computational calculations support the formation of P=O bonds during the oxidation steps. The computational calculations suggest that the thermocatalytic H_2O splitting occurs on the P atoms of doped graphene through a stepwise process involving an intermediate with a P-OH group and a H attached to a neighboring C atom and subsequent H_2 evolution, leading to the formation of P-O bonds.

Introduction

Among the most general ways to obtain graphene-related materials, the one starting with graphite that is submitted to deep chemical oxidation to graphite oxide, followed by subsequent exfoliation to graphene oxide (GO) and final chemical reduction provides a graphene material denoted as reduced graphene oxide (r-GO). r-GO is among the most widely studied graphene material because it can be prepared in a reliable way in gram scale (Scheme 1).[1-2]

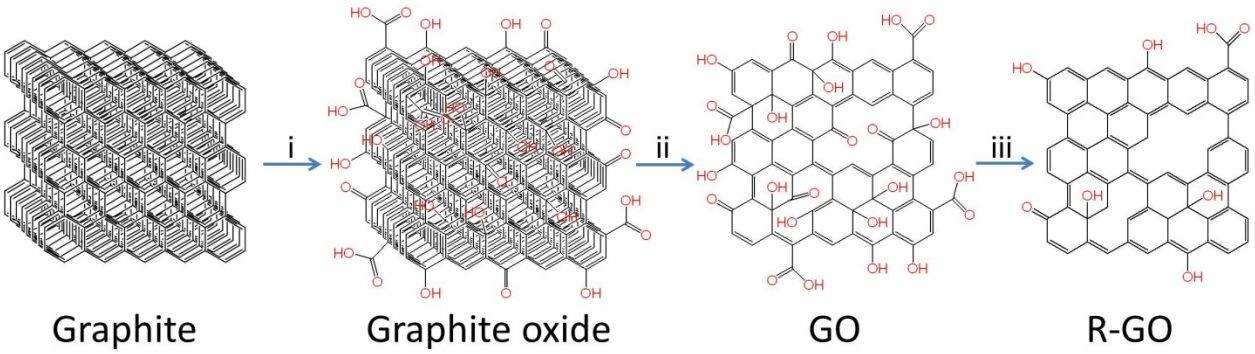

Scheme 1. Process of preparation of r-GO from graphite involving oxidation to graphite oxide and exfoliation to GO. (i) chemical oxidation, (ii) exfoliation and (iii) chemical reduction.

The above process to perform graphite exfoliation by conversion of graphene (G) into GO is based on the possibility to carry out with a certain degree of control the oxidation and reduction of G/GO increasing the oxygen content to above 50 wt.% from G to GO and, then, subsequently decrease this oxygen content to from 50 about 10 wt.% characteristic of r-GO. This ability to increase and decrease the oxygen content on G sheets is reminiscent of the so-called Mars van Krevelen oxidation/reduction of non stoichiometric transition metal oxides in where the oxygen content of the inorganic oxide can be varied to a certain extent, generally much lower than the one commented in the case of G/GO/r-GO.[3] This Mars van Krevelen mechanism has been, however, advantageously used to promote catalytic oxidations/reductions and, more related to the present work, this swing between two related materials with different oxygen content is at base of thermochemical cycles for water splitting or steam reforming.

In steam reforming, a substrate (S) promotes the reduction of water, resulting in the generation of hydrogen (Eq. 1) and substrate oxidation. If the oxidized form of the substrate, most frequently

inorganic oxides (normally ceria, perovskites or spinel ferrites) due to the required thermal stability (T = 1300 – 1500 ºC), can subsequently be thermally reduced by oxygen evolution (Eq. 2), then the two steps can serve to perform cyclically the overall water splitting.[4-5] It has been reported that one of the main challenges in thermochemical water reforming is the development of materials able to promote efficiently thermochemical transformations at low temperatures (< 1100 ºC), especially for large scale production.[5-7]

$$S + H_2O \rightarrow S_{ox.} + H_2 \qquad \text{Oxidation} \qquad \text{Eq. 1}$$

$$S_{ox.} \xrightarrow{\Delta} S + O_2 \qquad \text{Activation} \qquad \text{Eq. 2}$$

Considering that, as commented above, graphene and related materials can exhibit different oxygen content in a much larger percentage than inorganic metal oxides can do, it occurred to us that they could be used either as substrates for steam reforming (Eq.1) or even for the metal-free thermochemical overall water splitting (Eq. 1 and 2). The state-of-the-art materials for thermochemical water reforming have been limited to the use carbon-based materials (active carbons) as support of metals or metal alloys.[8-9] In the present article, however, it would be shown that while defective graphenes obtained from biomass undergo steam reforming generating hydrogen from water and becoming completely oxidized to CO_2, the presence of oxophilic P dopant on the G sheet changes completely the behavior of graphene decreasing considerably the generation of CO_2 in the steam reforming process. The P doping provide exceptional thermal stability to the G sheets in a similar way to the reported for N doped G.[10] Oxygen release has still to be achieved to reach a certain cycling in the thermochemical generation of H_2.

In the present study the thermochemical steam reforming of two different graphene materials, one obtained by pyrolysis of alginic acid and the other one the P-rich carbon residue from phytic acid pyrolysis would be compared. In a series of articles it has been shown that pyrolysis of alginic acid, a natural polysaccharide formed by the (1-4)-linkage of β-D-mannuronic and α-L-guluronic acids, renders a turbostratic graphitic carbon residue that can undergo easily exfoliation in a very high yield given rise to defective G.[11-14] The defects on this G material obtained from alginic acid consist in the presence of oxygenated functional groups, due to the presence of a residual oxygen content of about 10 %, as well as the presence of carbon vacancies and holes, among other possibilities. It has been shown that these defective Gs derived from alginate exhibit catalytic activity for a series of organic reactions promoted by these defects acting as catalytic sites.[11, 15] The properties and the performance of G from alginate is frequently similar to that of r-GO. Related to the present work, it has been recently reported that G from alginate can promote the aqueous phase reforming of glycerol at 250 ºC acting as catalyst (Eq. 3).[16] Control experiments in the absence of glycerol show that under these reaction conditions, no hydrogen or CO_2 is evolved from graphene, showing that Eq. 1 does not take place at 250 ºC in aqueous suspensions of Gs.[16]

$$C_3H_8O_3 + H_2O \rightarrow 3\,CO_2 + 7\,H_2 \qquad \text{Eq. 3}$$

Besides defective G from alginate and considering the possible influence that dopant elements as oxophylic centers can exhibit favoring hydrogen generation from water by capturing the oxygen atom, in the present study a P-rich doped graphitic carbon was prepared by pyrolysis of phytic acid (see structure in Fig. S1 in supplementary information).[17]

Phytic acid is one of the most ubiquitous natural molecules containing phosphorous. Among the different roles of phytic acid, the most important one is to act as reservoir of phosphate in biological systems, but it is also known that phytic acid can inhibit some enzymatic processes related to protein hydrolysis.[18] Phytic acid is abundant in the fibers of legumes and other grains. There is a precedent in the literature in where thermal decomposition of phytic acid was carried out at 500 ºC forming a carbonaceous residue that has catalytic activity to promote oxidation of hydrocarbons by oxygen.[19] In the present study pyrolysis of phytic acid was carried out at 900 ºC and subsequent exfoliation of the residue by sonication renders a dispersion whose characterization indicates that it corresponds to a P-doped defective graphene (Phy-G). This Phy-G material was used as catalyst for the thermochemical steam reforming of water, demonstrating a maximum H_2 generation per cycle of 21.6 μmol/min·g, working for over 20 consecutive cycles of activation and hydrolysis at 800 and 650 ºC, respectively. The lack of O_2 evolution during the activation steps indicates that Phy-G is undergoing gradual oxidation. Experimental and computational studies support that the thermocatalytic H_2O splitting occurs on the P centers of doped graphene through a stepwise process involving P-OH group intermediates and a H attached to a neighboring C atom, being the first step the rate-limiting one.

Experimental Methods

Sample Preparation

Phytic acid solution 50 % (w:w) in water (Aldrich) was directly used without further purification. The phytic acid solution was placed in a drier at 120 ºC and allowed to dry overnight. The dry residue was subsequently pyrolyzed at 900 ºC in Ar atmosphere for 2 h

increasing the temperature at 20 ºC/min and allowing to cool by equilibration with the ambient. The carbon residue was dispersed in ethanol and sonicated at 700 W for 3 h. Finally, the solid was recovered from the ethanol suspension by centrifugation and dried under vacuum at 40 ºC overnight.

Sample characterization

Raman spectra were collected with a Horiba Jobin Yvon-Labram HR UV-Visible-NIR (200-1,600 nm) Raman Microscope Spectrometer, using a 512 nm laser. The spectrum was collected averaging 10 scans at a resolution of 2 cm^{-1}

HRTEM images were recorded in a JEOL JEM 2100F under accelerating voltage of 200 kV. Samples were prepared by applying one drop of the suspended material in ethanol onto a carbon-coated copper TEM grid, and allowing them to dry at room temperature.

AFM measurements were conducted in contact mode in air at ambient temperature using a Veeco apparatus operating in tapping mode.

XP spectra were measured on a SPECS spectrometer equipped with a Phoibos 150 9MCD detector using a non-monochromatic X-ray source (Al and Mg) operating at 200 W. The samples were evacuated in the prechamber of the spectrometer at $1 \cdot 10^{-9}$ mbar. The measured intensity ratios of the components were obtained from the area of the corresponding peaks after nonlinear Shirley-type background subtraction and corrected by the transition function of the spectrometer.

NMR measurements were performed on a Bruker MSL 400 NMR spectrometer with a magnetic field strength of 9.4 T and a ^{31}P NMR frequency of 161.96 MHz. MAS rotation frequencies were 5 and 8 KHz, and proton decoupling was applied. For the measurements, a 90º pulse

acquire sequence with a 2.5 μs pulse length, a 5 μs dwell time, 1024 data points, and a 4 s recycle delay were used for accumulating 400 – 600 scans. Saturation effects were not detected under these conditions.

Thermocatalytic H_2 Evolution

Thermochemical cycles were performed in two units. One of them was a NETZSCH STA 449 Jupiter thermobalance equipped with an electric furnace suitable for the oxidation reaction at several Ar flow rates and water concentrations (maximum working temperature 1250 ºC).

Other thermochemical cycles were monitored in a tubular reactor placed inside an electric furnace as displayed in Fig. S2a in supplementary Information. In the experimental study, a fixed-bed reactor was used and the reactor characteristics allowed the control of the heating rate and temperature, enabling the determination of kinetic laws. Mullite tube was used for the activation and oxidation reactions, respectively. About 0.2 g of powder sample was placed in a Pt/Rh (90:10) crucible inside the tubular reactor (Fig. S2b in Supplementary Information). The sample was heated under a 100 mL min^{-1} Ar flow to the desired temperature at a rate of 40 ºC × min^{-1} and then held isothermally for some time. Steam for the hydrolysis step was generated by passing Ar through deionized water at 80 ºC.

The effluent gas was analysed by a gas chromatograph (Varian CP4900), equipped with a molecular sieve column and a TCD detector, which automatic sampling of gas aliquots from the reactor outlet every ca. 2 min. This apparatus allows the analysis and quantification of H_2, O_2, CO, CH_4, at each step to determine the efficiency of the process (Fig. S2a in Supplementary Information). Numerical integration of the obtained molar flow time curves provides the total amount of hydrogen evolved.

Computational Details

The potential energy calculations have been performed using spin polarized DFT with the VASP 5.4.1 code (Vienna ab-inito simulation program) developed at the Fakultät für Physik of the Universität Wien.[20] We use the projector augmented wave (PAW) scheme[21] with the Perdue-Burke-Ernzerhof (PBE)[22] exchange and correlation (xc)-functional and a plane-wave energy cutoff of 400 eV. The system is modeled by a hexagonal 5x5 unit cell containing 50 atoms with a P atom substituting a C atom (2% doping),[23] with an optimized C-C bond separation of 1.429 Å and a 14 Å separation between graphene sheets. Γ-point sampling of the reciprocal space has been used in the optimizations and the nudged elastic band (NEB)[24] method calculations. These have been used to locate the transition state structures, employing four images as in previous studies.[25-26] In the computations of the water splitting and phosphoric acid formation reaction energetics, the **k**-point density has been increased to 4×4×1, and the separation between graphene sheets to 22 Å and 26 Å. The interaction energies are determined as the energy difference between the adsorbate/substrate interacting configuration minus the configuration with the adsorbate and substrate components separated and non-interacting while both included within the unit cell. With this computational set-up, the water and dihydrogen with P-doped graphene interaction energies are -0.92 and -0.87 kcal mol^{-1}, respectively, in full agreement with previous data on undoped graphene.[27] The standard free energy corrections at 650°C include the vibrational contributions of the bonds that are broken and formed along the reaction coordinate and the vibrational, rotational and translational contributions of the free molecules. They have been estimated from gas-phase calculations at the PBE/6-311g** level (see more details in the Supplementary Information).

Results and discussion.

Sample characterization

Combustion chemical analysis indicates that the carbon content of Phy-G was of 41.8 wt %. X-Ray photoelectron spectroscopy (XPS) shows the presence of C, O and P in agreement with the composition of the phytic acid used as precursor (see Figure 1). Small amounts of N from impurities present in phytic acid were also detected in Phy-G. The atomic composition at the surface of the Phy-G sample determined by XPS was 74.7, 17.8, 5.4 and 1.1 % for C, O, P and N, respectively. This corresponds to a weight proportion of 65.71, 20.88, 12.27 and 1.13 wt% for C, O, P and N, respectively. These values give higher-than-expected C content in Phy-G in view of the combustion chemical analysis, indicating the preferential location of C at the outermost layers of the Phy-G particles. Deconvolution of the C 1s peak in the high resolution XPS shows the presence of three components that can be attributed to graphenic carbon (48.5 %), carbon bonded to oxygen (8.8 %) and carbon bonded to phosphorous (42.7 %) at binding energies of 284.5, 288.1 and 283.4 eV, respectively, similarly to previous reports of P-doped graphene.[28] Analysis of the O 1s peak indicates, on the other hand, also the presence of three different types of oxygen appearing at binding energy values of 529.8 (19.8 %), 533.8 (15 %) and 531.6 (65.2 %) eV that are attributable to two families of oxygen atoms bonded to carbon (C=O and C-O) and one oxygen type bonded to phosphorous (O=P-), respectively.[29-30] XPS also exhibits a peak for P 2p that can be deconvoluted in three components with binding energies of 131.8, 132.98 and 135.8 eV with relative percentages of 17.88, 9.14 and 72.98 %, respectively. The component at lower binding energy is attributable to phosphorous coordinated to carbon (P-CCC) while the components at higher energies (132.98 and 135.8 eV) are related to phosphonate and phosphate groups, respectively.

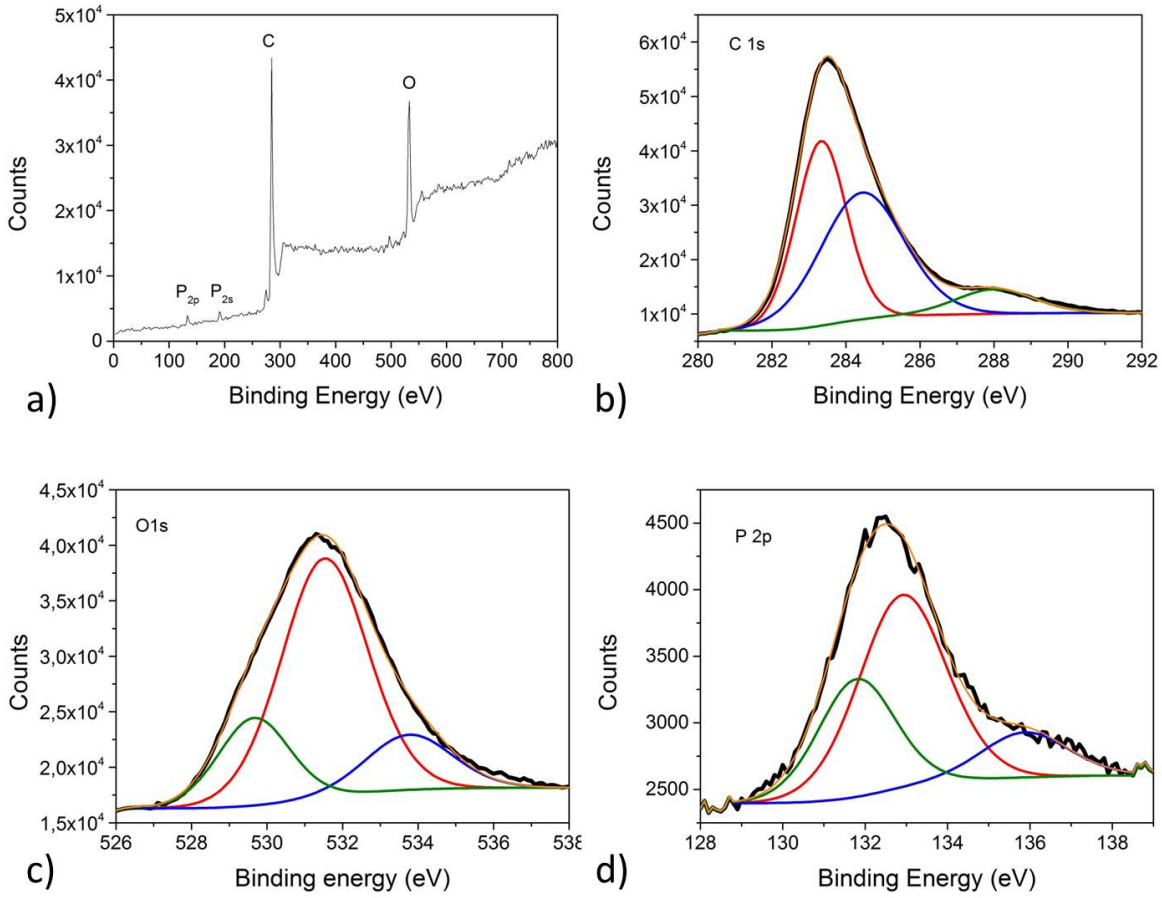

Figure 1. XPS survey spectrum (a) and C1s (b), O1s (c), P2p (d) high resolution peaks recorded for Phy-G, and their corresponding best deconvolution fits.

Further information on the type of P atoms present on the Phy-G material was obtained by solid state MAS 31P nuclear magnetic resonance (NMR) spectroscopy (Figure 2), that shows the presence of four peaks appearing at 29, -4, -13, -26 ppm, respectively. These 31P peaks can be assigned based on the literature to P atoms analogous to triphenylphosphine oxide (O=PPh3, expected value at + 28 ppm),[31] triphenylphosphine (PPh3, expected value at -5 ppm),[32-33] diphenylphosphate (O=P(OH)Ph2, expected value at -10.4 ppm)[34] and organic phosphanates

((OH)2(O)PPh, expected value at -10 ppm in PO4 terminal groups) respectively,[35-36] in good agreement with the deconvolution of the XPS P 2p peak that indicates the presence of various types of P, either lacking oxygen or bonded to one or more oxygen atoms. The morphology of Phy-G particles was observed by high resolution transmission electron microscopy (HRTEM) (Figure 3), whose high resolution images revealed the expected sheet morphology characteristic of 2D graphenic materials of several micrometers lateral size and exhibiting a high crystallinity with hexagonal arrangement characteristic of graphenic materials. In addition to those graphene sheets, the presence of amorphous nanometric particles showing a 3D morphology without any atomic arrangement or crystallinity were also observed as accompanying impurity on the Phy-G sample, probably associated to the formation of undefined P-containing carbon particles.

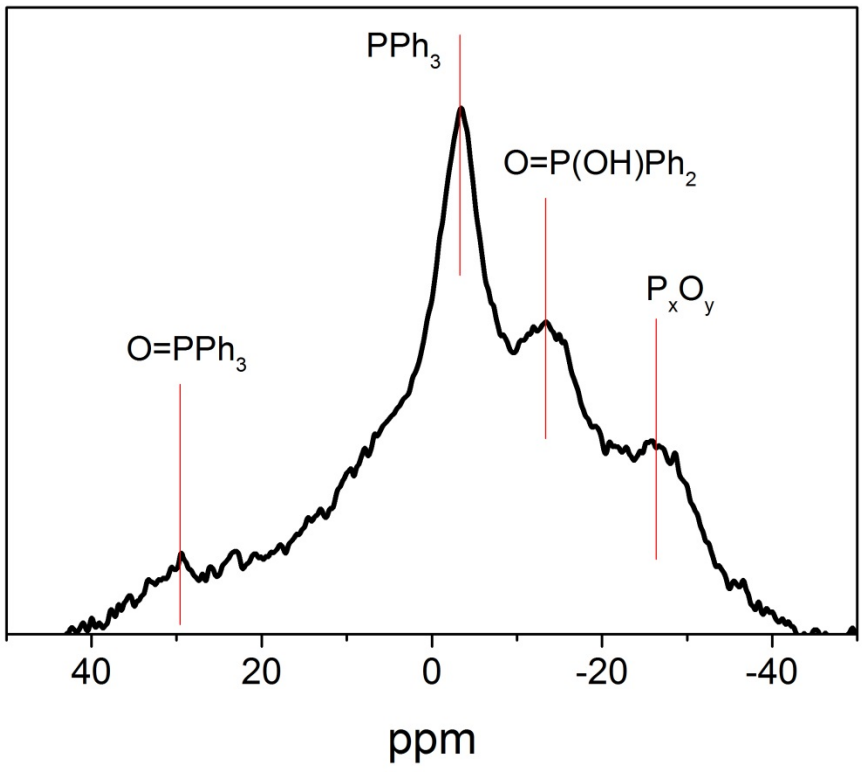

Figure 2. Solid state ^{31}P NMR spectrum of Phy-G, with indication of the assignment based on the literature. [31-34]

The preferential characteristic 2D morphology of Phy-G was confirmed by atomic force microscopy (AFM). The lateral size and height of Phy-G was measured after depositing a drop of Phy-G dispersion in ethanol on atomically flat mica substrate and allowing solvent evaporation. The 2D particles presented lateral dimensions between 3 and 8 μm with an average height of 2.5 nm, indicating that they correspond to few layers graphenic sheets. Figure 4 presents some AFM images corresponding to the 2D sheets and the nanometric particles as well as some measurements with subnanometric vertical resolution of the sheets. In order to discard that the 2D layers observed in the AFM images in Fig. 4 are due to the formation of solvent 2D films, as reported elsewhere,[37] Phy-G sample was prepared depositing a drop of the Phy-G dispersion in ethanol on a mica substrate and subsequent heating at 110 ^{0}C for 3 h prior AFM image acquisition (Fig. S3 in Supplementary Information).

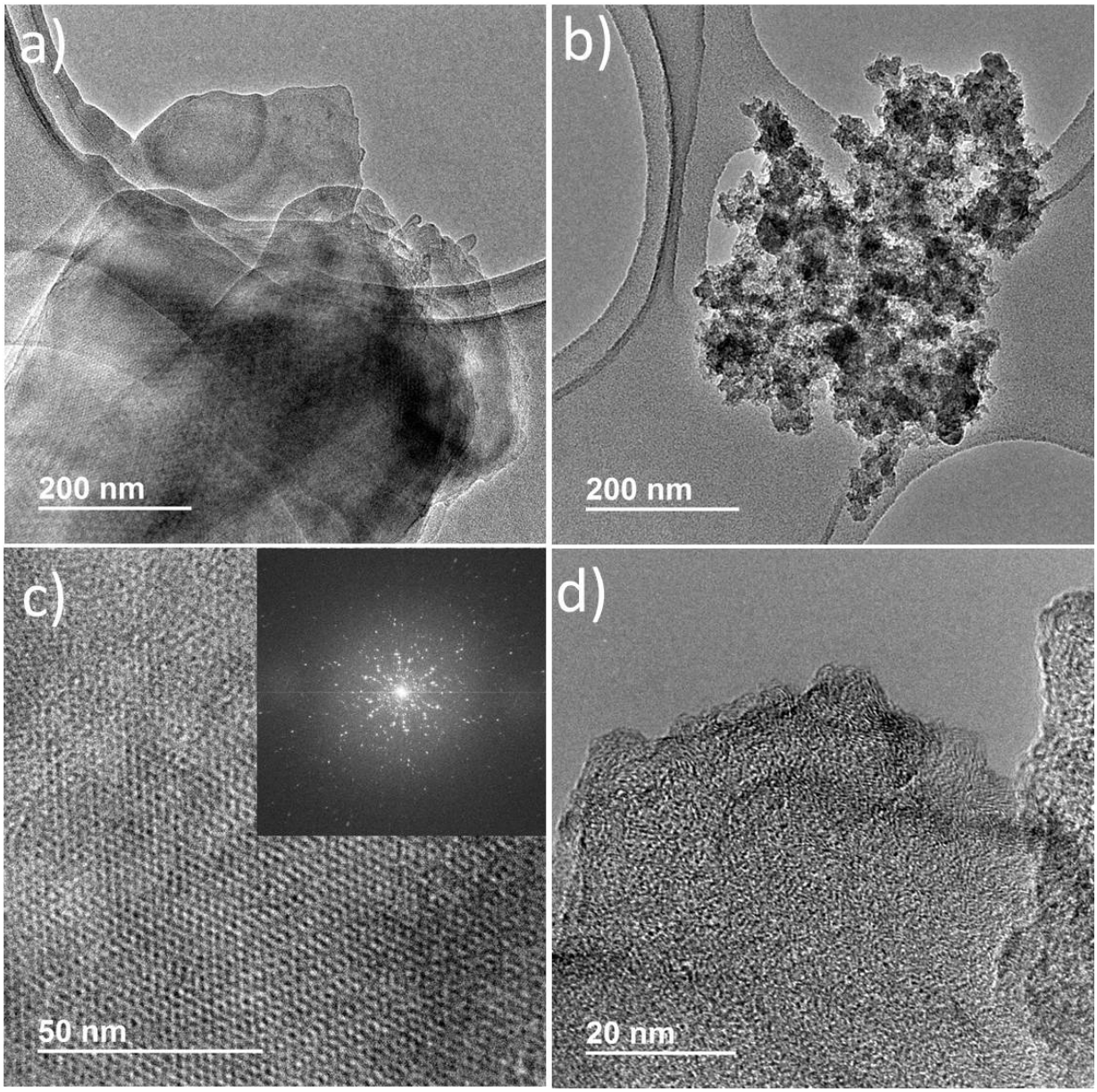

Figure 3. HRTEM images showing the different types of particles observed in the Phy-G samples. (a) Graphenic sheet of several micrometers exhibiting 2D laminar morphology. (b) Submicrometric particles with rough morphology. (c) Magnification of image (a) showing the spatial hexagonal arrangement. Inset shows electron diffraction pattern indicating the high crystallinity of the graphene sheets. (d) Magnification of image (b) for which no crystallinity was observed.

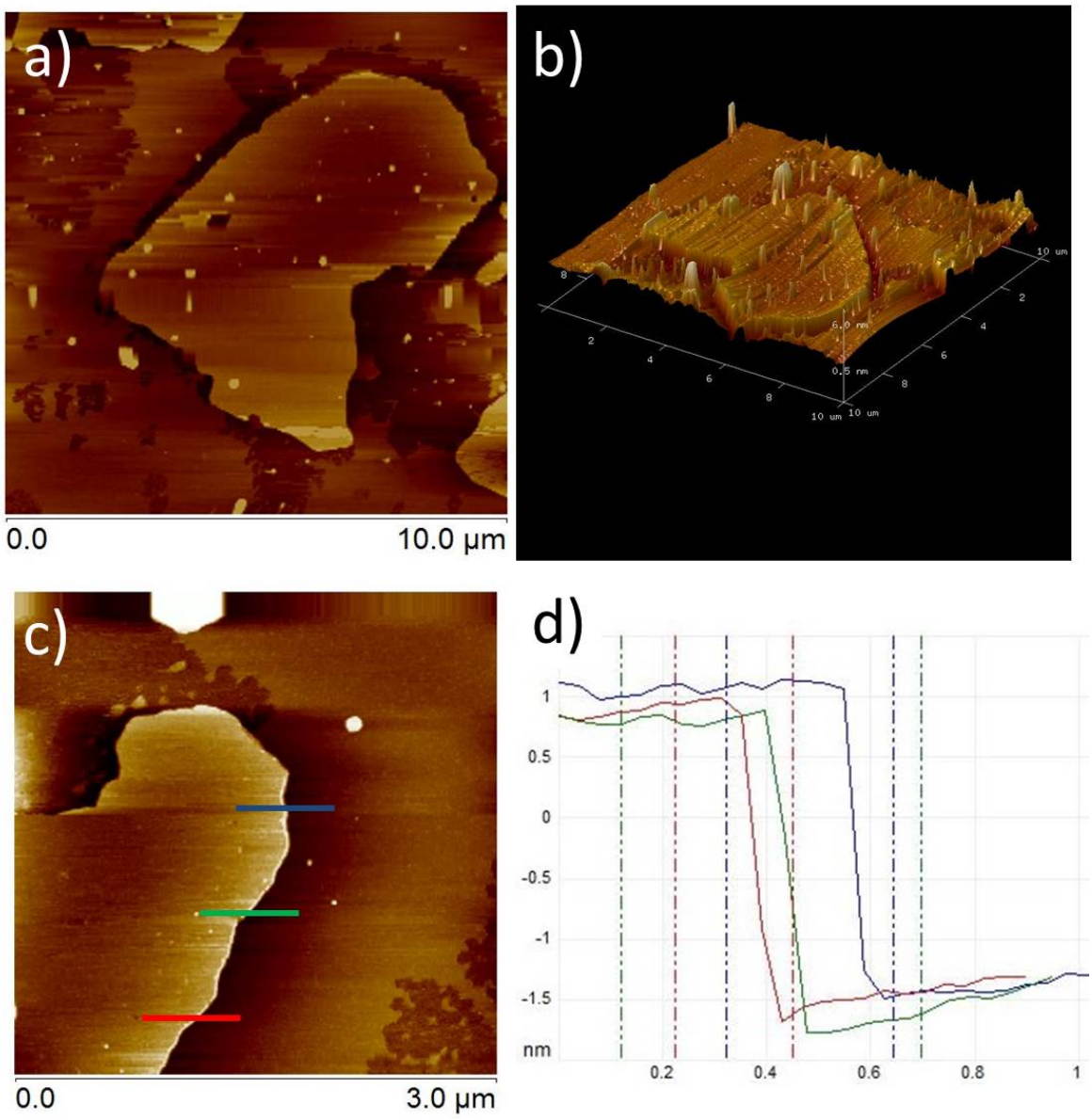

Figure 4. AFM images of Phy-G samples. (a) General wide field image of Phy-G samples showing a 2D sheet on which smaller particles are supported. (b) 3D image of a wide field region of the same Phy-G sample. (c) Image corresponding to a part of a 2D sheet, where the blue, green and red lines indicates the height measurements. (d) Height measurement along the lines indicated with the same colors in image (c).

The number of layers cannot be determined, since the thickness of a single Phy-G sheet is unknown. In the case of N-doped G, a thickness about 1 nm has estimated for a single layer[38] and similar thickness could be considered here. AFM also reveals the presence in lesser proportion of a second type of particles ranged in size from 50 to 500 nm accompanying the prevalent 2D sheets of nanometric thickness as observed by HRTEM.

The presence of defects on the Phy-G graphenic material and some quantitative indication of the density of these defects can be assessed by Raman spectroscopy (Figure 5). Raman spectrum of Phy-G exhibits the three 2D, G and D peaks characteristic of doped defective Gs appearing at 2700, 1600 and 1350 cm-1, respectively. The relative intensity of the G versus the D peak (I_G/I_D) was 1.19. This is a common value for other defective graphenes obtained by pyrolysis of polysaccharides[11] that also have somewhat higher I_G/I_D ratios than those reported for common r-GO of around 0.9.[39] Higher I_G/I_D ratios are generally indicative of lower defect density on the material. Further perusal of the Raman spectra of Phy-G Raman spectra shows a shoulder in the D band located at 1169 cm^{-1} as well as a peak in the low frequency region at 466 cm^{-1} that can be attributed to O-P-O bending of the phosphoric and phosphonate groups.

All together the present available data shows that, in agreement with earlier reports on the formation of defective graphenes by pyrolisis of some biomass compounds, pyrolysis of phytic acid at 900 ºC also results on the formation of a defective graphene containing P atoms grafted on the sheet having different coordination environments. It is expected that these P atoms located on the sheets of G can act as catalytic sites and oxophitic centers promoting water decomposition, particularly Eq. 1 in which oxygen becomes attached to the material resulting in the generation of hydrogen.

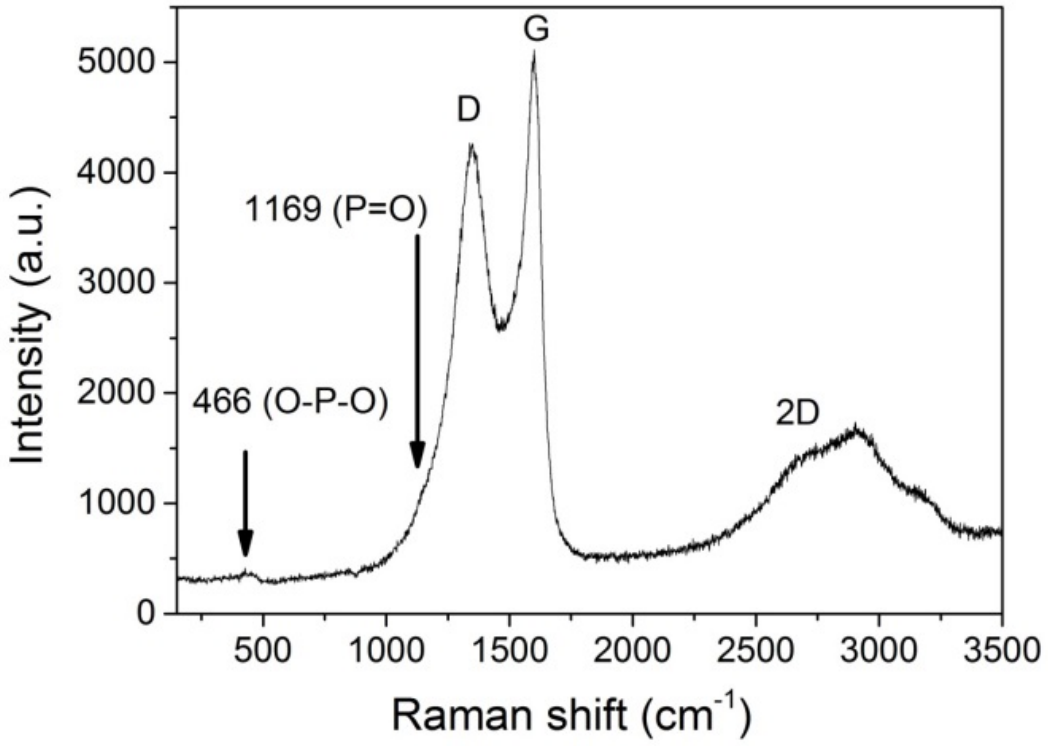

Figure 5. Raman spectrum of Phy-G sample indicating the position of the D, G, and 2D bands, as well as the location of some characteristics stretching bands corresponding to P-O bonds.

Steam Reforming

Thermochemical experiments were carried out using a tubular reactor placed inside an electric furnace containing Phy-G as displayed in Fig. S2a in supplementary information. Approximately 200 mg of the solid samples were loaded in a Pt/Rh crucible, and introduced in the tubular reactor (see Fig. S2b in supplementary information). Prior to starting the thermochemical H_2O splitting cycle, Phy-G sample was submitted to thermal activation at 850 ºC under vacuum for 4 h in order to remove adsorbed molecules and volatile impurities. Then, successive activation-

oxidation steps at 800 ºC under dry Ar and at 650 ºC under H_2O-saturated Ar atmosphere, respectively, corresponding to attempts to achieve Eq. 1 and 2, were carried out. The gases evolved during 21 consecutive activation-oxidation cycles were analyzed by GC chromatography, whereby evolution of H_2 as the main product accompanied by detectable amounts of CH_4 and CO, could be determined and quantified. Fig. 6 presents H_2 evolution profile during 21 consecutive cycles of activation-oxidation. As it can be observed there, H_2 was produced during oxidation steps (Eq. 1), obtaining from 21.6 μmol/$g_{Phy\text{-}G}$ in the first cycle to 5.5 μmol/min·$g_{Phy\text{-}G}$ in the last cycles. This evolution indicates a gradual fatigue of the Phy-G sample upon increasing the number of cycles. In contrast, the formation rate of CH_4 and CO, much lower than that of H_2, was found practically constant in every step of the cycle, regardless the temperature (800 or 650 ºC) and the presence or absence of H_2O (See Fig. S4 in Supplementary Information). The formation of these two gases appears, therefore, related to the continuous decomposition of Phy-G catalyst during the process. Thermogravimetric (TG) analysis of Phy-G during activation-oxidation cycles under the reaction conditions revealed a slight and continuous mass loss over time (Fig. S5 in Suplementary Information).

For comparison purposes defective G obtained from alginic acid pyrolysis at 900 ºC under Ar atmosphere was also submitted to activation-oxidation cycles under identical conditions as those of Phy-G. The G sample obtained from this biopolymer has been widely characterized in the literature,[11] and it has been reported that defective G obtained from this precursor contains a residual O content. In agreement with the reported data, XPS measurements revealed the presence on G of O in a proportion of 8.45 wt%.[11] Therefore, this defective G sample can be considered similar to the one obtained from phytic acid, although lacking P in its composition.

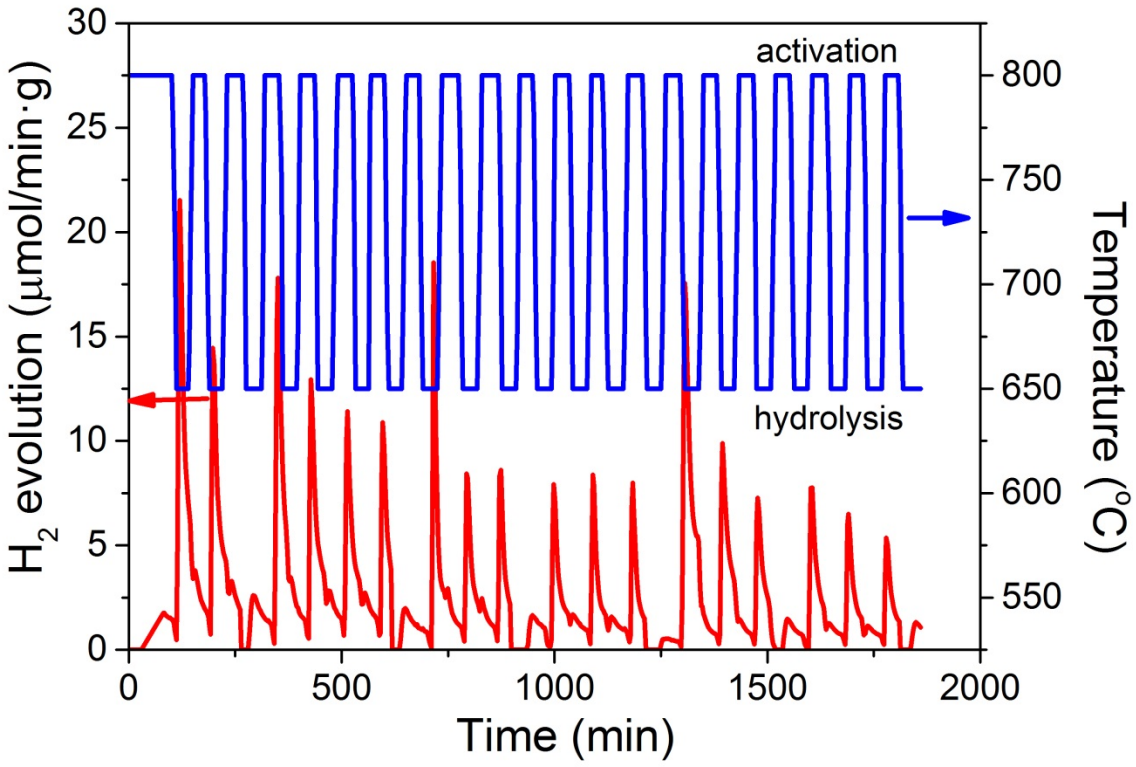

Figure 6. H_2 evolution upon 21 consecutive activation-oxidation cycles (red). The temperature cycles have been included in blue.

However, as it can be observed in the TG curve shown in Fig. S5, G obtained from alginic acid is not stable under the successive activation-oxidation cycles, and it decomposed completely in the first 10 cycles under the reductive conditions. Accordingly, G from alginate undergoes steam reforming under the conditions of hydrolysis step, becoming oxidized to CO_2, while H_2 is generated. Therefore, it is clear that P-doping changes significantly the behavior of the G sheet such that it becomes more stable with regard to H_2O oxidation. It has been also observed in the literature that dopand elements, such as N, can make active carbon more stable towards chemical

oxidation by nitric acid,[40] and a similar effect would be caused here by oxyphilic P atoms present on Phy-G.

Lack of O_2 evolution

It is worth noticing that evolution of O_2 was not detected in any step in these experiments either using Phy-G or G, indicating that Eq. 2 does not take place. However, since H_2 evolves in the hydrolysis steps, it is clear that the O atoms present in H_2O must remain attached in the Phy-G catalyst or could promote some decomposition. In order to address the nature of the oxygenated groups being formed on Phy-G, Raman spectroscopy and XPS analysis of the Phy-G catalyst after extensive use in the thermochemical H_2O reactions were carried out.

The XPS P 2p peak of Phy-G after its use in steam reforming and its best deconvolution fit are presented as Figure 7, that also provides a comparison with the P 2p peak of the fresh sample. The first information provided by XPS was a decrease in the proportion of P quantified by the decrease of the P/C atomic ratio from the initial 0.072 value for the fresh Phy-G material to the 0.021 ratio determined for the Phy-G sample after its use in the thermochemical H_2 generation from H_2O. Comparison of P 2p spectra of fresh and used Phy-G confirms a shift in P 2p peak of the used Phy-G towards higher binding energies, indicating the increasing presence of oxidized P in the catalyst composition. In addition, as it can be observed in Figure 7, the P 2p peak of Phy-G after reaction presents only two main components instead of three. In this case, the component at 132 eV related to P-C bond is no longer present, while components at 134 and 136 eV in a relative percentages of 74.5 and 25.5, respectively, are related to the formation of P-O bonds.

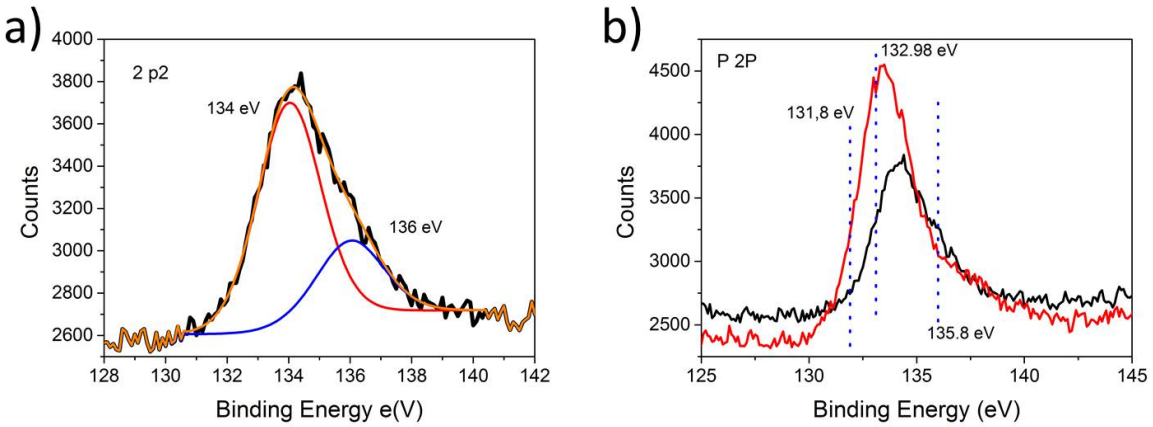

Figure 7. High resolution XPS P 2p peaks measured for Phy-G after reaction (a). (b) Comparison of the P 2p peak of Phy-G before (red) and after (black) its use in the thermolysis of H_2O. Dotted lines represent the maximum of the three components present in the P2p peak of fresh Phy-G.

Raman spectra of Phy-G before and after reaction have also been compared, and the results are shown in Fig. S6 in Supplementary Information. As can be observed in the high frequency region of the Raman spectrum, the 1169 cm^{-1} band related to P=O vibrations has grown in intensity after the Phy-G use in H_2 evolution reaction. In a similar way, the low frequency region of the Raman spectrum shows a weak 466 cm^{-1} band that has grown in intensity compared to fresh Phy-G sample and other peaks also related to P-O vibration modes, such as those appearing at 857 and 590 cm^{-1}. These data from Raman spectroscopy are in good agreement with the XPS data, showing that P atoms have undergone a transformation toward phosphate groups after the reaction increasing their level of P-O bonds.

In addition, the relative intensity of the G versus the D band due to the graphene lattice has also changed after reaction, being of 0.83. This value is similar to those reported for r-GO materials, indicating that not only the P atoms are being oxidized during reaction, but also the graphenic C structure increases its defect density, probably related to the detachment of P atoms and also to some oxidation as well.

The solid-state ^{31}P NMR spectra of fresh and used Phy-G have been similarly recorded and they are compared in Fig. S7 of the Supplementary Information. As it can be seen there, the contribution of peaks corresponding to triphenylphosphine and triphenylphosphine oxide has considerable decreased, while the peaks attributed to phosphate and other P oxide groups have undergone a notable increase in good agreement with the information provided by XP and Raman spectroscopies. Therefore, the incorporation of O atoms in P-doped G as phosphate groups is confirmed by three different techniques, and thus, the lack of O_2 gas in the stream can be attributed to the oxophilic nature of P and also to some degree of graphenic C oxidation during reaction. Observation of CH_4 and CO in the thermochemical cycles clearly indicates this gradual oxidation of G, since the most likely origin of CH_4 is methanation of CO_2.

Mechanism Discussion

Density functional theory calculations with the PBE functional (see Computational Details) have been carried out to explain the thermochemical H_2 evolution from H_2O on Phy-G. Similar reactivity studies have been carried out for the oxygen reduction reaction on P-doped graphene,[41-42] but not for steam reforming. Similar to these studies, we assume that the catalytic activity is provided by P atoms that substitute a single C atom on the graphene sheet, forming three P-C bonds, and model the catalytic centers on a periodic graphene sheet. This model is

consistent with our experimental ^{31}P NMR spectrum, which shows the presence of triphenylphosphine-like atoms (Figure 2), and with the experimental surface contents of 5.4 % (XPS). The latter corresponds to an average P-P distance of approximately 7.5 Å, which indicates that the catalytic effect will be provided by single P atoms. Given that the surface may also contain other defects whose distribution is not known, we opt for an idealized model with 2% P content (P-P distance 12.3 Å) that allows us to study the catalytic effect of an isolated P atom.

The computed mechanism supports that P atoms are the catalytic centers reacting with H_2O in a stepwise fashion, as shown in Figure 8a. Attempts to calculate a concerted mechanism of H_2 evolution and O attachment to the surface did not provide reasonable results. Note that for convenience, Figure 8 only represents the carbon atoms in the vicinity of the catalytic center. The calculated mechanism starts with a physisorbed water molecule (**R**). The first step consists of OH dissociation and simultaneous addition of the OH and H fragments to the P atom and a neighboring C site, respectively. It takes place through TS1 and leads to intermediate **I1**. The estimated barrier is 66.0 kcal/mol, and the step is endoergic by 40.1 kcal/mol. The second step is the dissociation of the second OH bond and formation of H_2 through TS2. This step involves, before the dissociation, a reorientation of the OH group leading to a second intermediate, **I2**, and it ends with the phosphonated product **P**. The energy barrier for this process, calculated from **I1**, is 50.2 kcal/mol. This suggests that the first step is the rate-determining one, while overall the steam reforming process is slightly endoergic by 5.3 kcal/mol. Other mechanisms are possible for the second, H_2 forming step, such as H diffusion on the surface and combination of two diffusing H atoms. However, the occurrence of these alternative mechanisms will not change the overall kinetics, since the first step remains to be the rate-determining one.

A possible mechanism for decomposition of the phosphonated product is shown in Figure 8b. It presents the calculated thermodynamics of three successive water additions to the P=O group, with simultaneous cleavage of one P-C bond in every step. This consecutive addition results in the detachment of a phosphoric acid molecule from the graphene sheet. This leaking of P atoms would be consistent with the experimental XPS that shows a loss of P in the process as well as with XPS and Raman spectra that indicate an increase in the P-O bond signals. The first two hydrolysis steps are endoergic by 23.1 and 26.8 kcal/mol, respectively, while the last step is endoergic by 39.6 kcal/mol. Following Eq. 2, an alternative to the hydrolysis would be P=O dissociation from P and regeneration of the initial catalyst. An accurate calculation of the barrier for this process is out of the scope of this work because it generates an oxygen atom which is difficult to treat computationally, but preliminary attempts with the current methodology yield an approximate estimate for the process of 80-100 kcal/mol uphill, showing that it is not viable.

Overall, the calculated energetics for H_2 generation are consistent with a mechanism where H_2O and H_2 reach an equilibrium during the hydrolysis cycles (see **Eq. 1** and **Fig. 7**), with gradual decomposition of the catalytic centers. In agreement with the available experimental data, calculations indicate that hydrolysis of the P=O center to phosphoric acid is preferred compared to regeneration of the catalyst and O_2 evolution, consistent with the lack of observation of this gas.

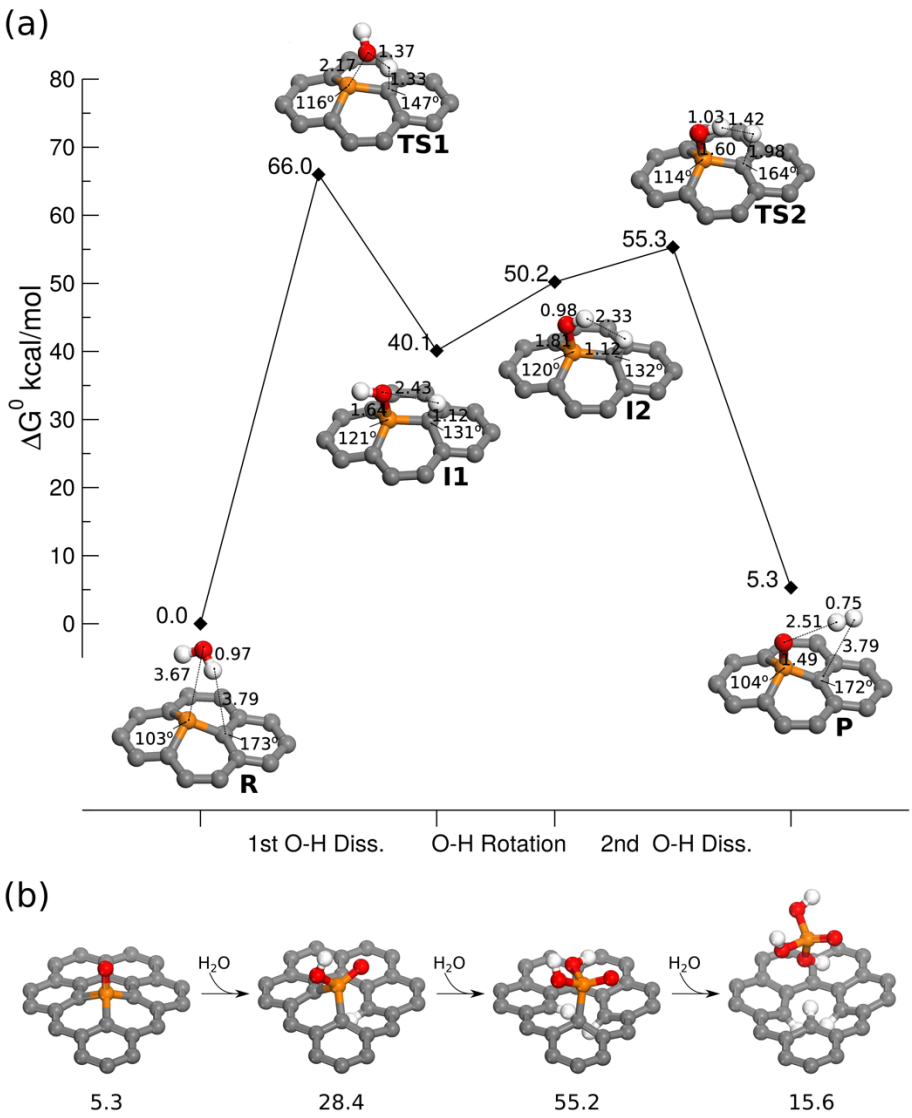

Fig. 8. (a) Calculated PBE standard free energy profile (kcal/mol) for the stepwise thermochemical water splitting reaction on P-doped graphene (2 %). The approximate transition structures TS1 and TS2 are the highest points on the NEB profiles (see Computational Details). The structures include the most significant bond lengths in Å and angles in °. (b) Calculated PBE free energy in kcal/mol (relative to the **R** structure) for the intermediates formed in three successive hydrolysis steps (addition of a H_2O molecule and cleavage of a P-C bond at every step) resulting in formation of phosphoric acid. Note that in both figures only the carbon atoms of the unit cell in the vicinity of the catalytic center are displayed.

In conclusion it has been shown that defective G obtained from biomass pyrolysis undergoes steam reforming at temperatures above 400 ºC forming H_2 and CO_2. Grafting of P atoms on the G sheet increases considerably its stability under conditions of steam reforming. A graphenic material doped with P was obtained by pyrolysis of phytic acid. Characterization of this material shows that together with the expected P-doped G, other nanoparticulated component is also present in much lesser proportions. Although the stability of Phy-G is notably higher than that of G and H_2 evolution is observed, no oxygen evolution could be achieved under the conditions tested. It seems that oxygen becomes too strongly attached to P atoms and also some degree of oxidation of the graphenic material to CO and CO_2 (converted to CH_4) is occurring. The computational calculations suggest that the thermocatalytic H_2O splitting occurs on the P atoms of doped graphene throgh a stepwise process involving an intermediate with a P-OH group and a H attached to a neighboring C atom. Subsequent H_2 evolution forms P=O. The first step is the rate-limiting one. The results are in line with the Sabatier principle, which states that if the interaction between the substrate and the catalyst is too strong, the product fails to dissociate from the catalyst, leading to a drop in efficiency. In the present case, the product does not dissociate completely from the catalyst because the P=O bond is too strong to allow for dissociation of atomic O. This results in hydrolysis and decomposition of the catalytic sites. Therefore, the search for a doped G that could promote the thermochemical water splitting due to the good balance between oxyphilicity, but moderate bond strength with the O should still continue.

Supporting Information.

The supporting information is available free of charge on the ACS Publications Website at DOI:

- Figure S1, Structure of phytic acid; Figure S2, Digital images of the experimental set up; Figure S3, CH_4 and CO evolution; Figure S4, TG analysis of Phy-G and defective G; Figure S5, Raman spectra of Phy-G after and before reaction; Figure S6, Solid ^{31}P NMR spectra of Phy-G bofre and after reaction. Details of free energy correction calculations. (PDF)

AUTHOR INFORMATION

*Hermenegildo García**,** Tel:. +34 96 387 78 07**,** E-mail: hgarcia@qim.upv.es

*Lluís Blancafort, Tel.: +34 972 41 88 06, E-mail: lluis.blancafort@udg.edu

Author Contributions

J.A. prepared and characterized the materials and wrote part of the manuscript; P.C. performed XPS measurements; A.V. performed the thermochemical experiments; A. M. performed the theoretical calculations; L.B. supervised the theoretical calculations and wrote part of the manuscript; H.G. supervised the research and wrote most of the manuscript. All the authors discussed the results and corrected the article draft.

ACKNOWLEDGMENT

J.A. and H.G. thank financial support by the Spanish Ministry of Economy and Competitiveness (Severo Ochoa SEV2016-0683, GRAPAS and CTQ2015-69563-CO2-1), Generalitat Valenciana (Prometeo 2017-083). JA also thanks UPV for postdoctoral scholarship. A.V. is grateful to National Plan for Scientific and Technical Research and Innovation 2013-2016 (ENE2015-71254-C3-2-R) since part of this work have been carried out within ARROPAR-CEX project. L.

B. and A. M. thank financial support by the Ministry of Economy and Competitiveness (CTQ2015-69363-P). We thank Mr. Pere Creus for carrying out some of the calculations. A.M. Thanks financial support by the Departament d'Innovació, Universitats i Empresa (DIUE), Generalitat de Catalunya (Project 2017SGR348). Calculations were carried out at the Red Española de Supercomputación (projects QCM-2017-3-0038 and QCM-2018-0037).

REFERENCES

1. Hummers, W. S.; Offeman, R. E., Preparation of Graphitic Oxide. *J. Am. Chem. Soc.***1958,** *80* (6), 1339-1339.
2. Stankovich, S.; Dikin, D. A.; Piner, R. D.; Kohlhaas, K. A.; Kleinhammes, A.; Jia, Y.; Wu, Y.; Nguyen, S. T.; Ruoff, R. S., Synthesis of graphene-based nanosheets via chemical reduction of exfoliated graphite oxide. *Carbon* **2007,** *45* (7), 1558-1565.
3. Mars, P.; van Krevelen, D. W., Oxidations carried out by means of vanadium oxide catalysts. *Chem. Eng. Sci.* **1954,** *3*, 41-59.
4. Nakamura, T., Hydrogen production from water utilizing solar heat at high temperatures. *Solar Energy* **1977,** *19* (5), 467-475.
5. Zhai, S.; Rojas, J.; Ahlborg, N.; Lim, K.; Toney, M. F.; Jin, H.; Chueh, W. C.; Majumdar, A., The use of poly-cation oxides to lower the temperature of two-step thermochemical water splitting. *Energy Environ.Sci.* **2018,** *11* (8), 2172-2178.
6. Piatkowski, N.; Wieckert, C.; Weimer, A. W.; Steinfeld, A., Solar-driven gasification of carbonaceous feedstock—a review. *Energy Environ.Sci.* **2011,** *4* (1), 73-82.
7. Zeng, K.; Gauthier, D.; Soria, J.; Mazza, G.; Flamant, G., Solar pyrolysis of carbonaceous feedstocks: A review. *Solar Energy* **2017,** *156*, 73-92.
8. Sano, T.; Hasegawa, N.; Tsuji, M.; Tamaura, Y., A carbon-bearing nickel(II) ferrite: a tailor-made solid reactant for two-step thermochemical water splitting at 300 °C. *J.Mat.Chem.* **1996,** *6* (4), 605-609.
9. Singhania, A.; Bhaskarwar, A. N., Performance of Activated-Carbon-Supported Ni, Co, and Ni–Co Catalysts for Hydrogen Iodide Decomposition in a Thermochemical Water-Splitting Sulfur–Iodine Cycle. *Energy Technol.* **2018,** *6* (6), 1104-1111.
10. Ajay, K.; Abhijit, G.; Pagona, P., Thermal stability study of nitrogen functionalities in a graphene network. *J.Phys. Condens. Matter* **2012,** *24* (23), 235503.
11. Trandafir, M. M.; Florea, M.; Neaţu, F.; Primo, A.; Parvulescu, V. I.; García, H., Graphene from Alginate Pyrolysis as a Metal-Free Catalyst for Hydrogenation of Nitro Compounds. *ChemSusChem* **2016,** *9* (13), 1565-1569.
12. Lavorato, C.; Primo, A.; Molinari, R.; García, H., Natural Alginate as a Graphene Precursor and Template in the Synthesis of Nanoparticulate Ceria/Graphene Water Oxidation Photocatalysts. *ACS Catalysis* **2014,** *4* (2), 497-504.
13. Atienzar, P.; Primo, A.; Lavorato, C.; Molinari, R.; García, H., Preparation of Graphene Quantum Dots from Pyrolyzed Alginate. *Langmuir* **2013,** *29* (20), 6141-6146.

14. Primo, A.; Forneli, A.; Corma, A.; García, H., From Biomass Wastes to Highly Efficient CO2 Adsorbents: Graphitisation of Chitosan and Alginate Biopolymers. *ChemSusChem* **2012,** *5* (11), 2207-2214.
15. Primo, A.; Neatu, F.; Florea, M.; Parvulescu, V.; Garcia, H., Graphenes in the absence of metals as carbocatalysts for selective acetylene hydrogenation and alkene hydrogenation. *Nat. Commun.* **2014,** *5*, 5291.
16. Esteve-Adell, I.; Crapart, B.; Primo, A.; Serp, P.; Garcia, H., Aqueous phase reforming of glycerol using doped graphenes as metal-free catalysts. *Green Chem.* **2017,** *19* (13), 3061-3068.
17. Zhang, J.; Qu, L.; Shi, G.; Liu, J.; Chen, J.; Dai, L., N,P-Codoped Carbon Networks as Efficient Metal-free Bifunctional Catalysts for Oxygen Reduction and Hydrogen Evolution Reactions. *Angew. Chem. Int. Ed.* **2016,** *55* (6), 2230-2234.
18. Mikulski, D.; Kłosowski, G., Phytic acid concentration in selected raw materials and analysis of its hydrolysis rate with the use of microbial phytases during the mashing process. *Journal of the Institute of Brewing* **2015,** *121* (2), 213-218.
19. Patel, M. A.; Luo, F.; Khoshi, M. R.; Rabie, E.; Zhang, Q.; Flach, C. R.; Mendelsohn, R.; Garfunkel, E.; Szostak, M.; He, H., P-Doped Porous Carbon as Metal Free Catalysts for Selective Aerobic Oxidation with an Unexpected Mechanism. *ACS Nano* **2016,** *10* (2), 2305-2315.
20. Kresse, G.; Furthmüller, J., *Phys. Rev. B* **1996,** *54*, 11169.
21. Kresse, G.; Joubert, D., From ultrasoft pseudopotentials to the projector augmented-wave method. *Phys. Rev. B* **1999,** *59* (3), 1758-1775.
22. Perdew, J. P.; Burke, K.; Ernzerhof, M., Generalized gradient approximation made simple. *Phys. Rev. Lett.* **1996,** *77* (18), 3865-3868.
23. Yang, N.; Zheng, X. Q.; Li, L.; Li, J.; Wei, Z. D., Influence of Phosphorus Configuration on Electronic Structure and Oxygen Reduction Reactions of Phosphorus-Doped Graphene. *J.Phy. Chem. C* **2017,** *121* (35), 19321-19328.
24. Sheppard, D.; Xiao, P. H.; Chemelewski, W.; Johnson, D. D.; Henkelman, G., A generalized solid-state nudged elastic band method. *J. Chem. Phys.* **2012,** *136* (7).
25. Migani, A.; Blancafort, L., Excitonic Interfacial Proton-Coupled Electron Transfer Mechanism in the Photocatalytic Oxidation of Methanol to Formaldehyde on TiO2(110). *J. Am. Chem.Soc.* **2016,** *138* (49), 16165-16173.
26. Migani, A.; Blancafort, L., What Controls Photocatalytic Water Oxidation on Rutile TiO2(110) under Ultra-High-Vacuum Conditions? *J. Am. Chem. Soc.* **2017,** *139* (34), 11845-11856.
27. Al-Hamdani, Y. S.; Alfe, D.; Michaelides, A., How strongly do hydrogen and water molecules stick to carbon nanomaterials? *J.Chem. Phys.* **2017,** *146* (9).
28. Latorre-Sánchez, M.; Primo, A.; García, H., P-Doped Graphene Obtained by Pyrolysis of Modified Alginate as a Photocatalyst for Hydrogen Generation from Water–Methanol Mixtures. *Angew. Chem. Int. Ed.* **2013,** *52* (45), 11813-11816.
29. Liu, Z.-W.; Peng, F.; Wang, H.-J.; Yu, H.; Zheng, W.-X.; Yang, J., Phosphorus-Doped Graphite Layers with High Electrocatalytic Activity for the O2 Reduction in an Alkaline Medium. *Angew.Chem. Int.Ed.* **2011,** *50* (14), 3257-3261.
30. Niu, F.; Tao, L.-M.; Deng, Y.-C.; Wang, Q.-H.; Song, W.-G., Phosphorus doped graphene nanosheets for room temperature NH3 sensing. *New J. Chem.* **2014,** *38* (6), 2269-2272.
31. Gutmann, T.; Bonnefille, E.; Breitzke, H.; Debouttiere, P.-J.; Philippot, K.; Poteau, R.; Buntkowsky, G.; Chaudret, B., Investigation of the surface chemistry of phosphine-stabilized

ruthenium nanoparticles - an advanced solid-state NMR study. *Phys. Chem. Chem. Phys.* **2013,** *15* (40), 17383-17394.
32. Tan, M.; Ishikuro, Y.; Hosoi, Y.; Yamane, N.; Ai, P.; Zhang, P.; Yang, G.; Wu, M.; Yang, R.; Tsubaki, N., PPh3 functionalized Rh/rGO catalyst for heterogeneous hydroformylation: Bifunctional reduction of graphene oxide by organic ligand. *Chem. Eng. J.***2017,** *330*, 863-869.
33. Shin, J.; Bertoia, J.; Czerwinski, K. R.; Bae, C., A new homogeneous polymer support based on syndiotactic polystyrene and its application in palladium-catalyzed Suzuki-Miyaura cross-coupling reactions. *Green Chem.* **2009,** *11* (10), 1576-1580.
34. Johnson, B. B.; Ivanov, A. V.; Antzutkin, O. N.; Forsling, W., 31P Nuclear Magnetic Resonance Study of the Adsorption of Phosphate and Phenyl Phosphates on γ-Al2O3. *Langmuir* **2002,** *18* (4), 1104-1111.
35. Hupfer, M.; Gtichter, R.; Ruegger, R. R., Polyphosphate in lake sediments: 31P NMR spectroscopy as a tool for its identification. *Limnology and Oceanography* **1995,** *40* (3), 610-617.
36. http://www.nmrnotes.org/NMRPages/refcomps.html http://www.nmrnotes.org/NMRPages/refcomps.html.
37. Zheng, Y.; Su, C.; Lu, J.; Loh, K. P., Room-Temperature Ice Growth on Graphite Seeded by Nano-Graphene Oxide. *Angew. Chem. Int. Ed.* **2013,** *52* (33), 8708-8712.
38. Primo, A.; Atienzar, P.; Sanchez, E.; Delgado, J. M.; Garcia, H., From biomass wastes to large-area, high-quality, N-doped graphene: catalyst-free carbonization of chitosan coatings on arbitrary substrates. *Chem. Commun.***2012,** *48* (74), 9254-9256.
39. Ok-Kyung, P.; Yong-Mun, C.; Jun Yeon, H.; Cheol-Min, Y.; Tea-Wook, K.; Nam-Ho, Y.; Hye Young, K.; Joong Hee, L.; Bon-Cheol, K.; Munju, G., Defect healing of reduced graphene oxide via intramolecular cross-dehydrogenative coupling. *Nanotechnology* **2013,** *24* (18), 185604.
40. Lathouder, K. M.; Crezee, E., Kapteijn, F. and Moulijn, J. A. (2008). Carbon Monoliths in Catalysis. In *Carbon Materials for Catalysis*. (eds P.Serp and J.L. Figueiredo).
41. Zhang, X.; Lu, Z.; Fu, Z.; Tang, Y.; Ma, D.; Yang, Z., The mechanisms of oxygen reduction reaction on phosphorus doped graphene: A first-principles study. *J.Power Sources* **2015,** *276*, 222-229.
42. Yang, N.; Zheng, X.; Li, L.; Li, J.; Wei, Z., Influence of Phosphorus Configuration on Electronic Structure and Oxygen Reduction Reactions of Phosphorus-Doped Graphene. *J.Phys. Chem. C* **2017,** *121* (35), 19321-19328.

SYNOPSIS

This works relates the preparation of P-doped graphene from phytic acid and evaluates its performance in thermochemical water reforming at mild conditions.

TOC/Abstract graphic

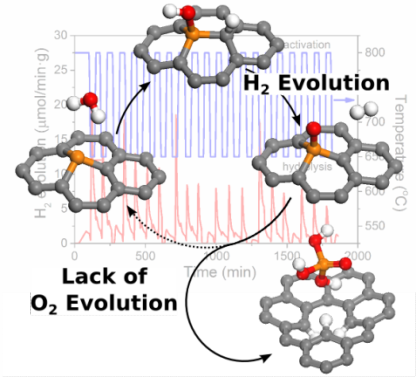
H_2 Evolution
Lack of
O_2 Evolution
Time (min)